Materials & Design 238 (2024) 112679

Contents lists available at ScienceDirect

Materials & Design

journal homepage: www.elsevier.com/locate/matdes

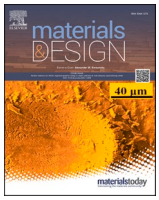

Thermodynamic modelling assisted three-stage solid state synthesis of high purity β-$Ca_3(PO_4)_2$

Sana Elbashir *, Markus Broström, Nils Skoglund

Umeå University, Department of Applied Physics and Electronics, Thermochemical Energy Conversion Laboratory, SE 901 87 Umeå, Sweden

ARTICLE INFO

Keywords:
β-TCP
Calcium phosphate
Thermodynamics
Solid state synthesis
FTIR
Raman
Rietveld refinement

ABSTRACT

A three-stage solid state synthesis assisted by thermodynamic modelling was developed to prepare highly pure (>99 %) beta tricalcium phosphate (β-TCP) powder. The optimal synthesis temperature was experimentally determined to be 1000 °C in good agreement with the theoretical calculations. The synthesis design described here has substantially improved the product quality and eliminated the presence of secondary phosphate phases compared to one- and two-stage methods investigated in this work. A comprehensive characterization of the material's structural, vibrational, and morphological characteristics was conducted. Rietveld refinement of the X-ray diffraction data confirmed the high purity of the samples. The crystal structure of the prepared β-TCP was determined and the refined unit cell parameters agreed well with the reference values. From infrared and Raman spectral analyses, the characteristics of β-TCP were observed and discussed in details. Furthermore, the morphology and elemental composition of the products were examined and found to be homogenous and impurity free. The reproducibility of the material was scrutinized and showed no significant data variations. Using our three-stage synthesis method, it is possible to produce β-TCP powder of high purity with consistent repeatability.

1. Introduction

Calcium phosphates (CPs) have gained increasing attention over the last decades [1–3]. Their unique physiochemical properties rendered them attractive materials for various applications in the biomedical, optical, environmental and industrial fields [4–6]. In the medical field, for example, CPs are extensively used for bone repair and tooth replacement owing to their excellent biocompatibility [7,8]. While in photonics applications, CPs are used as luminophores that host variety of luminescent cations [4,9,10]. In addition, the structural nature of CPs promotes their use as effective sorbents of contaminants in environmental applications [11,12]. Moreover, CPs are often used as a phosphorus source in the production of fertilizers, food and feed additives, detergents, and many other industrial chemicals [6,13,14].

Tricalcium phosphate $Ca_3(PO_4)_2$ (TCP) is one of the most important CPs and receives extensive interest in the scientific and medical communities due to its advantageous properties [2]. TCP is typically formed at high temperatures, above 800 °C with a characteristic Ca/P molar ratio of 1.5 [15]. In general, there are three polymorphs of TCP; beta (β), alpha (α) and alpha prime (α') [15]. β-phase is stable at room temperature (25 °C) up to 1125 °C and considered to be the most stable phase of TCP. The other two phases i.e., α and α', are metastable at atmospheric conditions and exist as stable phases only at temperatures above 1125 °C and 1430 °C, respectively [15–17]. β-TCP is commonly known as whitlockite (natural phosphate mineral) owing to the similarity of their crystal structure [18]. The whitlockite crystal structure has a large unit cell consisting of many different anionic and cationic sites. Atomic substitution in the cationic sites can take place without distortion of the whitlockite structure [18,19]. Moreover, in β-TCP, the cationic substitution of Ca^{2+} by other cations is a well-established strategy for tailoring its properties to the intended applications [8,20–25]. Hence, full understanding of β-TCP crystal structure and its characteristics is critical for maximizing the potential of this important material. To achieve that, synthesizing β-TCP powder of high quality is crucial.

Different methods for β-TCP preparation are reported in the literature, including solid state, wet precipitation and sol–gel synthesis routes [26–29]. The low-temperature routes seem to be favoured in some disciplines more than the high-temperature methods. However, based on the phase equilibria of the $CaO–P_2O_5$ system, β-TCP does not form at low

* Corresponding author.
E-mail address: sana.elbashir@umu.se (S. Elbashir).

https://doi.org/10.1016/j.matdes.2024.112679
Received 16 November 2023; Received in revised form 15 January 2024; Accepted 16 January 2024
Available online 17 January 2024

temperatures [30]. Therefore, additional high-temperature treatment (sintering) is always required to transform the product into β-TCP [28,29,31]. Moreover, the wet chemical methods are often complicated and require continuous monitoring of many parameters e.g., pH [32,33]. Deviation from the optimal pH typically leads to incomplete reaction or precipitation resulting in impurity phases. Likewise, using precipitated amorphous calcium phosphates for the production of β-TCP via thermal conversion is complex due to their metastability in aqueous solutions [34]. The crystallization of these amorphous phosphates is thus, not yet well understood. Conversely, the solid state method produces β-TCP of higher crystallinity [35]. The elevated temperature promotes the crystallization process and reduces crystal defects. However, particles agglomeration under high temperature is a common problem. This agglomeration leads to product heterogeneity and often required extensive milling which in turns can be a source of contamination [28]. In addition to the conventional routes, other solid state synthesis methods, such as high-pressure, spark plasma, and laser sintering have been employed for the synthesis of CPs including β-TCP [36–38]. These advanced techniques are robust and time efficient, however, there are many associated drawbacks, such as high cost and energy usage. Furthermore, these techniques are only successful on a small scale and implementation on a large scale is still a challenge [36]. Another challenge in the synthesis of β-TCP at both high and low temperature is the presence of secondary phosphate phases e.g., hydroxyapatite ($Ca_5(PO_4)_3OH$, HA) and calcium pyrophosphate ($Ca_2P_2O_7$) in the final product [15,39]. The presence of these phases is an unfavourable outcome especially if the prepared material is intended for biomedical applications [40]. These impurity phases can affect the biological, physical, and chemical properties of β-TCP in those applications [34]. Nevertheless, the best method of synthesizing high-quality β-TCP is a subject for improvement. One possible way to optimize the synthesis of single phase β-TCP is to perform thermodynamic equilibrium calculations that predict the formation reaction of β-TCP. These calculations enable one to investigate the reaction pathways under various conditions and to identify the possible impurity phases. Also, provide prediction of key information such as optimal temperature range at which single phase β-TCP can exist.

In this work we present an efficient three-stage solid state synthesis method for preparing high purity (>99 %) β-TCP powder with consistent reproducibility. The aim is to provide a reliable synthesis strategy/design that can overcome the common practical problems associated with the synthesis of this important material. Furthermore, this work introduces for the first time the use of thermodynamic modelling to assist the experimental design of β-TCP synthesis. The experimental synthesis parameters were intensively examined and the synthesis design is thoroughly described to provide the know-how knowledge necessary to produce high quality material. The prepared materials were extensively characterized using powder X-ray diffraction (XRD) combined with Rietveld refinement, Fourier transform infrared spectroscopy (FTIR), Raman spectroscopy, inductively coupled plasma optical emission spectroscopy (ICP-OES), and scanning electron microscopy coupled with energy dispersive X-ray spectroscopy (SEM-EDS). These comprehensive analyses aimed to provide deep insights into structural, vibrational, and morphological characteristics of β-TCP.

2. Material and methods

2.1. Thermodynamic equilibrium calculations

Thermodynamic equilibrium calculations for β-TCP formation were performed using FactSage 8.2 Software (Thermfact Ltd., Canada and GTT-Technologies, Germany) [41]. This software utilizes the Gibbs energy minimization approach to calculate the phase equilibria and thermal stability of the formed phases. The calculations were performed in the Equilib module and the databases used were FactPS and FToxid [42,43]. The reaction of stoichiometric quantities of $CaCO_3$ and $(NH_4)_2HPO_4$ was assumed to take place at atmospheric pressure. The investigated temperature range was 100–1900 °C, with a step size (ΔT) of 20 °C. Phase transitions were considered in the model. The theoretical calculations predicted the optimum synthesis conditions i.e., temperature for obtaining a single phase β-TCP that was implemented in the experimental design. It should be noted that, thermodynamic equilibrium calculations do not consider reaction kinetics. Thus, the theoretical and experimental results may slightly disagree.

2.2. Starting materials and synthesis design

Pure crystalline β-TCP was prepared using a three-stage solid state method. The synthesis protocol was designed based on both thermodynamic equilibrium calculations and reported work [44]. $CaCO_3$ (99.95 %, purity, Merck-Sigma Aldrich), $(NH_4)_2HPO_4$ (≥99 %, purity, Merck-Sigma Aldrich) were dried at 105 °C for 24 h and then used to prepare the material. The drying of $(NH_4)_2HPO_4$ was critical to obtain the desired Ca/P ratio of 1.5 in the resulting product. Stoichiometric amounts of the reactants were mixed, ground using an agate mortar and pestle and used according to the following overall chemical reaction:

$$3CaCO_3(s) + 2(NH_4)_2\,HPO_4(s) \rightarrow \beta\text{-}Ca_3(PO_4)_2(s) + 4NH_3(g) + 3H_2O(g) + 3CO_2(g) \quad (1)$$

The powder mixture was then placed in a Pt crucible and heated in a muffle furnace in three-stages. The three-stage strategy can be described by the following chemical reactions:

$$2(NH_4)_2\,HPO_4(s) \rightarrow 2NH_4\,H_2PO_4(s) + 2NH_3(g)\uparrow \rightarrow 2H_3PO_4(l) + 2NH_3(g) \quad (2)$$

$$3CaCO_3(s) \rightarrow 3CaO(s) + 3CO_2(g) \quad (3)$$

$$3CaO(s) + 2H_3PO_4(l) \rightarrow \beta\text{-}Ca_3(PO_4)_2(s) + 3H_2O(g) \quad (4)$$

It is worthily noting that, $CaCO_3$ partially reacts with H_3PO_4 in an acid-base reaction [17]. This reaction leads to formation of calcium phosphate intermediates during stage 1–2. These reaction intermediates react further with CaO at stage 3. Thus, H_3PO_4 is consumed before stage 3. For brevity, these reaction intermediates are not shown in equations (1)–(4), instead H_3PO_4 is kept as phosphorus reactant to balance Eq. (4).

Fig. 1 below shows a scheme of the three-stage synthesis strategy. As can be seen in the schematic diagram, preheating at 350 °C for 6 h (Eq. (2)) was performed in the first stage to allow complete decomposition and evaporation of NH_3 and H_2O gases [45]. The direct decomposition of the ammonia-based reagent into H_3PO_4 in solid state reaction as well as its non-corrosive nature [46] promote its use as an attractive P precursor. The second heating stage at 680 °C for 6 h (Eq. (3)) was intended to initiate the decomposition of the carbonate group, CO_3, which promotes efficient reaction to form the final product in stage 3. The resulting powder from the first two stages was then hydraulically pressed at a pressure of 160 MPa into a pellet with a diameter of 10 mm. Finally, the pellet was heated to 1000 °C and kept at this temperature for 20 h to achieve single phase β-TCP (Eq. (4)). A heating rate of 3 °C/min was used throughout the experiments.

After the synthesis time elapsed, the sample was left inside the furnace to cool down to room temperature. The final product was ground into fine powder and stored in a desiccator prior to the analytical measurements.

The three-stage heating strategy was crucial to avoid stickiness of the intermediate liquids onto the crucible walls, which leads to particles agglomeration and formation of heterogenous products. The synthesis protocol was conducted three times to ensure the reproducibility of the synthesized material. It is worth noting that, this three-stage synthesis design was developed after several attempts using one-stage (direct) and two-stage synthesis approaches. The results of those trials are elaborated in details below.

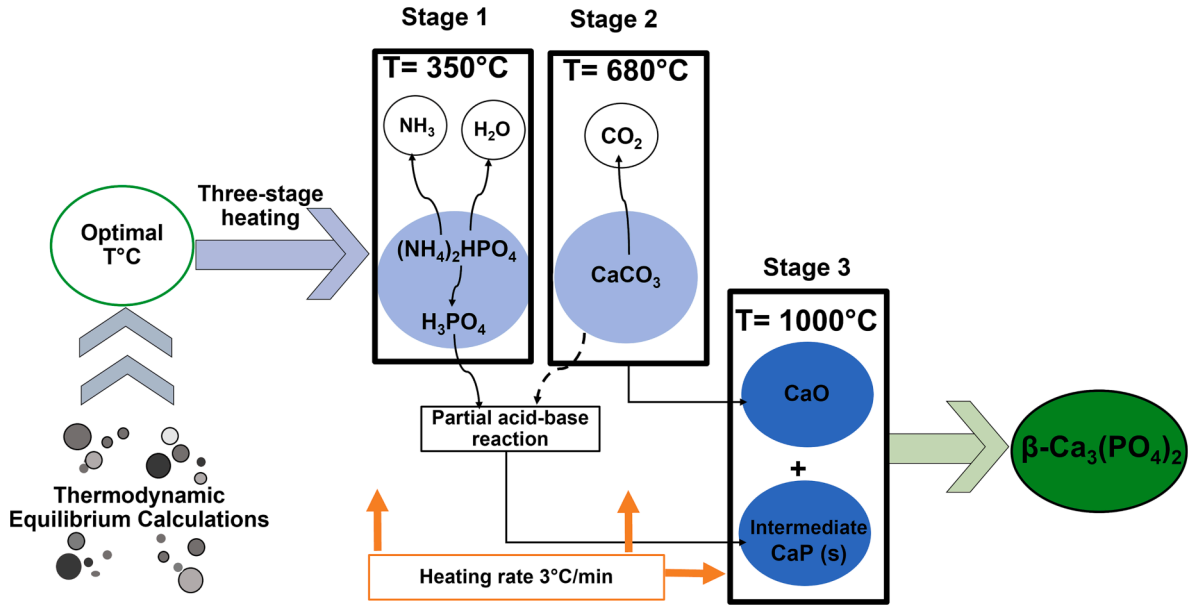

Fig. 1. A scheme of the three-stage solid state synthesis of pure β-TCP.

2.3. Analytical methods

The qualitative and quantitative phase analyses of the samples were performed using XRD analysis and Rietveld refinement. A Bruker D8 Advance (Bruker AXS, Germany) diffractometer with Cu-Kα radiation source (λ = 1.5406 Å) operating at 40 kV and 40 mA, and equipped with a Våntec-1 detector was used for the measurements. The diffraction patterns were collected in (θ–θ) mode in the 2θ range of 10–70° with a step size of 0.008° and scan speed of 1°/min. DIFFRAC.EVA software and PDF4 + database were used for phase identification [47,48]. Rietveld refinement was performed using DIFFRAC.TOPAS 4.2 software [49]. Moreover, FTIR measurements were performed using a Bruker IFS 66v/S (Bruker Optics, Germany) in the frequency range of 4000–400 cm^{-1} with 128 scans min^{-1} acquisition and a resolution of 4 cm^{-1}. Prior to the FTIR measurements, the samples were ground and mixed with potassium bromide (KBr). Bruker BRAVO spectrometer (Bruker Optics GmbH, Germany) equipped with two NIR diode lasers (Duo Laser™) at wavelengths 785 and 852 nm was used to record Raman spectra in the range of 300–3000 cm^{-1} with 128 scans min^{-1} acquisition and a resolution of 4 cm^{-1}. A ZEISS Merlin field emission scanning electron microscope (FE-SEM) (Carl ZEISS, Germany) was used to study the morphology of the samples. For the imaging, the samples were coated with a layer of Pt of 2 nm thickness. A ZEISS EVO LS-15 variable pressure microscope (Carl ZEISS, Germany) operating at ETH = 15 kV was used

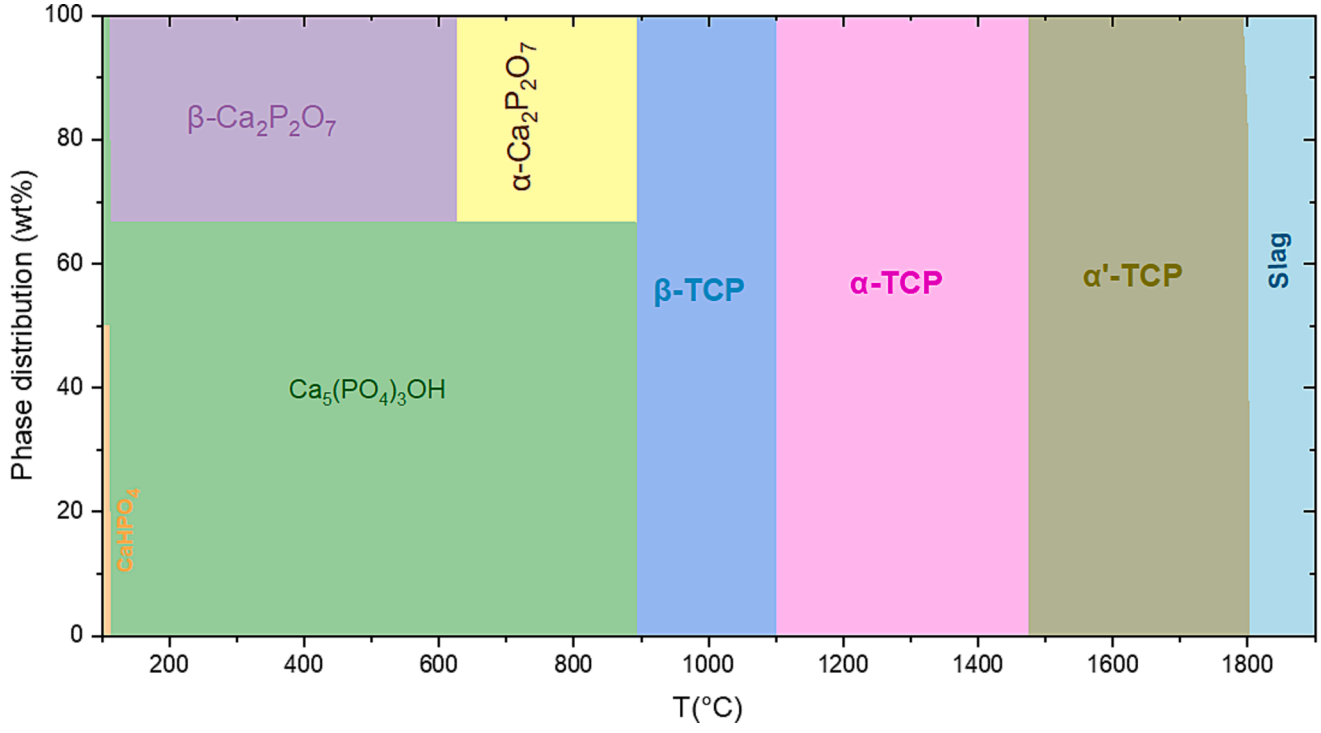

Fig. 2. Condensed phases from thermochemical equilibrium calculations for β-TCP formation at temperature range of 100–1900 °C.

for the EDS elemental analysis. An Agilent 5800 ICP-OES (Agilent Technologies Inc., USA) was used to determine the bulk elemental composition of the samples. A standard aqua regia dissolution method was used to prepare the powders for the analysis.

3. Results and discussion

3.1. Thermodynamic equilibrium calculations for β-TCP formation

The results obtained from the thermodynamic equilibrium calculations for β-TCP formation are presented in Fig. 2 above. The stable condensed phases, comprising solid compounds and solid solutions (Slag in Fig. 2), are the focus of this discussion. Gas phases and intermediary liquids were included in the calculations to permit decomposition of the reactants (not shown here).

As discussed above, the calculations were performed to model the overall synthesis reaction (Eq. (1)) and the reaction is assumed to be irreversible as gaseous species are evaporated. As shown in Fig. 2, the initial phases, $CaHPO_4$, $Ca_5(PO_4)_3OH$ and $Ca_2P_2O_7$ form at $\leq$ 100 °C. The first phase is predicted to decompose at 110 °C, while the latter two dominate the phase composition up to around 895 °C. The β-TCP phase is formed at a temperature range of 900–1100 °C and only stable in this range. Below this temperature, a multiphase solid solution is formed. Above 1100 °C, α-TCP starts to dominate and undergoes phase transition into α'- TCP polymorph at around 1475 °C. From the model, temperature above 1800 °C leads to complete decomposition of TCP phases that transform into molten slag. These results agree well with thermodynamic assessments of phase equilibria in the $CaO–P_2O_5$ system that are reported in the literature [15,39]. Based on these calculations, a temperature exceeding 900 °C is required to ensure a successful synthesis of single phase pure β-TCP.

3.2. Effect of synthesis design on the product purity

Series of synthesis experiments were conducted to determine the optimum design for producing pure β-TCP powders. During the experiments, several trials including one, two and three-stage synthesis procedures were investigated. According to the phase diagram of Fig. 2, the ideal synthesis temperature is predicted to be $>$ 900 °C. From our experimental investigations, it was concluded that a temperature of 1000 °C is optimal to produce $>$ 99 % pure β-TCP. Table 1 below summarizes the synthesis design, the experimental conditions and the products purity when using the optimal T = 1000 °C. Phase identification and quantification were performed using XRD and Rietveld analyses. Reference structures from ICSD (FIZ Karlsruhe, Germany) of identified compounds used for Rietveld refinement: β-TCP (PDF Card-01-090-0977) [50], α-TCP (PDF Card-04-022-5804) [51], HA (PDF Card-00-055-0592) [52], and β-$Ca_2P_2O_7$ (PDF Card-04-009-8733) [53].

As can be noticed from Table 1, using direct one-stage synthesis procedure resulted in low quality products consisting of heterogeneous mixture of β-TCP in combination with HA and β-$Ca_2P_2O_7$. The two-stage procedure resulted in slightly improved products with purity ranging from 86 % to 88 %. However, the second heating step at 680 °C was not sufficient to obtain pure material. So, an additional heating step at 350 °C was necessary to facilitate the homogeneous decomposition and interatomic diffusion of the precursors.

Furthermore, various samples were prepared at temperatures of 900 °C, and 1100 °C. It was found that at temperature 900 °C, the resulted products were heterogenous mixtures of β-TCP, HA and β-$Ca_2P_2O_7$. While at 1100 °C, the α-TCP phase was dominating over β-TCP in the final products. These results agree well with the thermodynamic calculations shown in Fig. 2.

Additionally, other synthesis parameters such as reaction time and heating rate were also investigated. Briefly, higher heating rates (5, 7, and 10 °C/min) led to the formation of poor-quality products. The rapid decomposition of the precursors is believed to induce their interaction with the Pt crucible surface. Likewise, shorter reaction times led to incomplete formation of the target compound, while longer reaction time promotes the formation of α-TCP phase at 1000 °C. From the results, the separation of heating stages is believed to facilitate the solid–solid interface and diffusion of ions in the active solids, which in turns, promote the nucleation of the pure product [54]. Also, applying pressure (hydraulic pressing) prior to the final heating stage increases the contact area of the activate phases and hence, influence the quality of the end product [55]. Based on our results; the procedure described here can minimize the common challenges in the high temperature routes such as heterogeneous formation of undesirable phases commonly observed during the synthesis of the material [56]. This synthesis strategy can be efficiently implemented in structural studies concerning β-TCP such as solid solubility (doping) of different cations in the phosphate matrix at high temperature.

3.3. XRD and Rietveld refinement of the pure β-TCP

The purity of the prepared materials was examined using XRD and Rietveld refinement as described above. Here, the structure determination of a representative pure β-TCP sample (TCP-3S-3) prepared using the three-stage protocol and its crystal structure are discussed in detail. The model structure reported by Liu et al (PDF Card-01–090-0977) was found to be a suitable starting point in the refinement [50]. The instrumental and experimental parameters; scale factor, background, zero shift and peak profile parameters were first refined. The peak

Table 1
Synthesis design, experimental conditions and purity of the products.

Synthesis design	Sample name	T(°C)/stage	Time(h)/stage	Sample Purity (wt%)	Impurity phases (wt%)	R-values	
One-stage	TCP-IS-1	1000	20	72.53(6)	HA: 2.55(5) β-$Ca_2P_2O_7$: 24.90(9)	R_{exp}:1.65 % R_{wp}:4.45 %	R_p:3.42 % GOF:2.69
One-stage	TCP-IS-2	1000	20	58.10(6)	HA:16.76(1) β-$Ca_2P_2O_7$: 25.13(3)	R_{exp}:2.40 % R_{wp}: 5.75 %	R_p:4.20 % GOF:2.40
One-stage	TCP-IS-3	1000	20	63.80(6)	HA:13.90(5) β-$Ca_2P_2O_7$: 22.28(9)	R_{exp}:1.79 % R_{wp}:6.56 %	R_p:4.90 % GOF:3.67
Two-stage	TCP-2S-1	680, 1000	6, 20	88.37(6)	HA: 3.96(9) β-$Ca_2P_2O_7$: 7.65(5)	R_{exp}:2.23 % R_{wp}:4.17 %	R_p:3.15 % GOF:1.87
Two-stage	TCP-2S-2	680, 1000	6, 20	87.32(5)	HA: 3.01(9) β-$Ca_2P_2O_7$: 9.65(7)	R_{exp}:1.97 % R_{wp}:6.42 %	R_p: 4.71 % GOF: 3.25
Two-stage	TCP-2S-3	680, 1000	6, 20	86.10(3)	HA: 2.47(8) β-$Ca_2P_2O_7$: 11.41(9)	R_{exp}:2.51 % R_{wp}: 4.80 %	R_p: 3.71 % GOF: 1.91
Three-stage	TCP-3S-1	350, 680, 1000	6, 6, 20	99.38(1)	HA: 0.39(8) α-TCP: 0.22(1)	R_{exp}:3.51 % R_{wp}: 7.15 %	R_p: 5.26 % GOF: 2.04
Three-stage	TCP-3S-2	350, 680, 1000	6, 6, 20	99.78(8)	HA: 0.12(9) α-TCP: 0.08(3)	R_{exp}:1.76 % R_{wp}: 5.08 %	R_p: 3.75 % GOF: 2.89
Three-stage	TCP-3S-3	350, 680, 1000	6, 6, 20	99.80(3)	α-TCP: 0.19(7) HA: 0.00(0)	R_{exp}:2.23 % R_{wp}: 4.86 %	R_p: 3.70 % GOF: 2.18

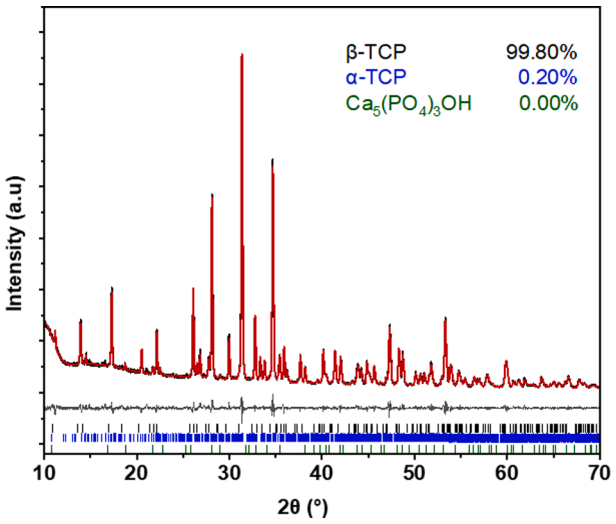

Fig. 3. Rietveld refinement plot of XRD pattern of the prepared material (TCP-3S-3). The observed pattern is shown in black, calculated pattern in red and difference line in grey. (For interpretation of the references to colour in this figure legend, the reader is referred to the web version of this article.)

profile parameters were refined using Pseudo-Voight functions. The unit cell parameters, site occupancy and thermal displacement parameters were refined later in the refinement. The obtained β-TCP crystalized in a trigonal system (rhombohedral) with hexagonal setting, space group R3c and Z = 21. The average unit cell parameters for the triplicates were determined to be a = b = 10.431 ± 0.007 Å, c = 37.376 ± 0.020 Å, α = β = 90°, γ = 120°, and unit cell volume = 3521.555 ± 6.322 Å^3. These refined unit cell parameters are consistent with the reported values in literature [44,50]. Also, the obtained R-factors as shown in Table 1 are well below the commonly accepted limits of a good refinement indicating the reliability of the model [57]. Nevertheless, the graphical result is of great importance in the evaluation of the refinement. Fig. 3 above shows the Rietveld refinement plot of the prepared material (TCP-3S-3).

The observed (black), calculated (red) patterns and difference line (grey) are depicted in the figure. The observed and calculated patterns show excellent agreement as demonstrated by the difference line. All observed peaks are sharp and well-defined signifying the high crystallinity of the material.

In general, β-TCP structure can be described by two columns along the c-axis of the unit cell, column A and column B. The β-TCP unit cell is illustrated in Fig. 4 below and the accommodated atoms are displayed as polyhedra along the c axis. Column A (Fig. 4b) consists of parallel layers of P (1) –Ca (4) –Ca (5) while column B (Fig. 4c) contains layers of Ca (1) –Ca (2) –Ca (3) –P (2) –P (3). Each column A is surrounded by six columns B and each column B is typically surrounded by two columns A in the unit cell [44].

Moreover, Ca sites have different coordination of eight-fold for Ca (1), Ca (2), and Ca (3) and six-fold for Ca (4) and Ca (5). These crystallographic differences between the cationic sites cause slight structural distortion of the P tetrahedra [44].

3.4. Vibrational spectra of β-TCP

FTIR and Raman techniques were used as complementary techniques to XRD and Rietveld refinement to provide structural information on the molecular level. Fig. 5 shows representative FTIR and Raman spectra of the prepared material (TCP-3S-3) in the range of 400–1400 cm^{-1} and 300–1500 cm^{-1}, respectively. The bands attributable to the internal vibration modes of PO_4^{3-} are observed in the 400–600 cm^{-1} and 900–1200 cm^{-1} ranges in the FTIR spectrum and shown in Fig. 5a. The bands in the 410–480 cm^{-1} range is assigned to the in-plane bending ν_2 of O–P–O, while the out-plane bending ν_4 are evident in the range 550–610 cm^{-1} [58]. The absorption bands that observed in the 900–1200 cm^{-1} range are ascribed to the symmetric stretching ν_1 and the antisymmetric stretching ν_3 as illustrated in Fig. 5.a. In theory, $\nu_3 > \nu_1$ and $\nu_4 > \nu_2$ for molecules with tetrahedron geometry like PO_4^{3-} [59]. This trend is observed in the recorded IR spectrum as shown in Fig. 5a.

The Raman spectrum of the prepared material is shown in Fig. 5b. The symmetric (in-plane) ν_2 and asymmetric (out-plane) ν_4 bending bands are observed in the region 400–700 cm^{-1}. At 900–1100 cm^{-1}, the strong Raman bands belongs to the symmetric stretching mode ν_1 and the weak bands at around 1100 cm^{-1} are assigned to asymmetric stretching ν_3 of PO_4^{3-} [60]. Table 2 summarises the observed vibrational bands in FTIR and Raman spectra in comparison to theoretical vibrational bands of free PO_4^{3-} ion calculated based on the group theory.

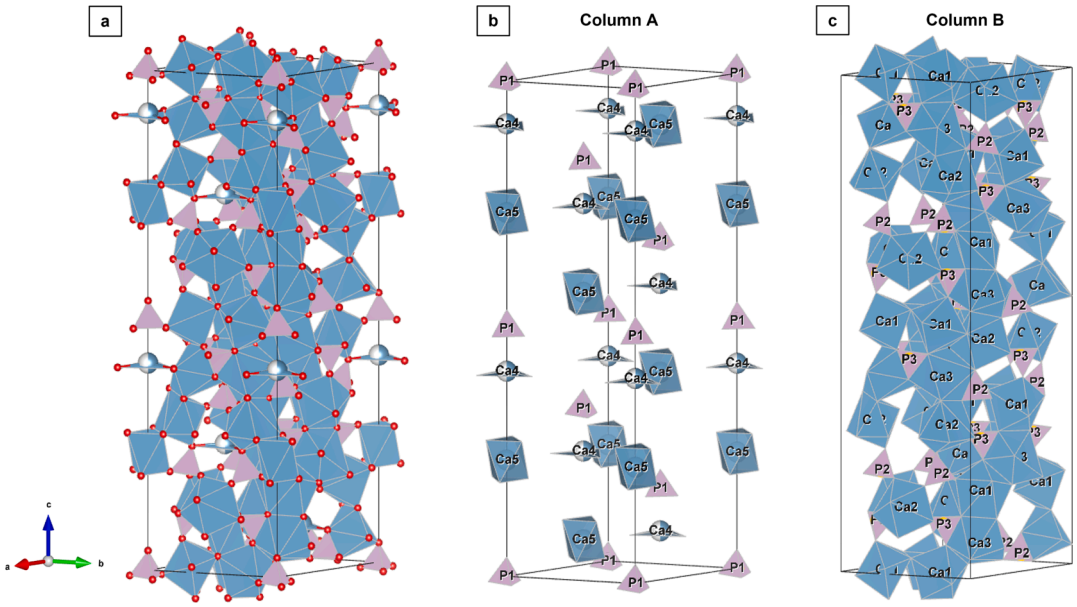

Fig. 4. Visualization of the β-TCP crystal structure. a) the hexagonal unit cell along the c axis. The unit cell composed of b) column A with parallel layers of P1–Ca4–Ca5 and c) column B with parallel layers of Ca1–Ca2–Ca3–P2–P3 along the c axis.

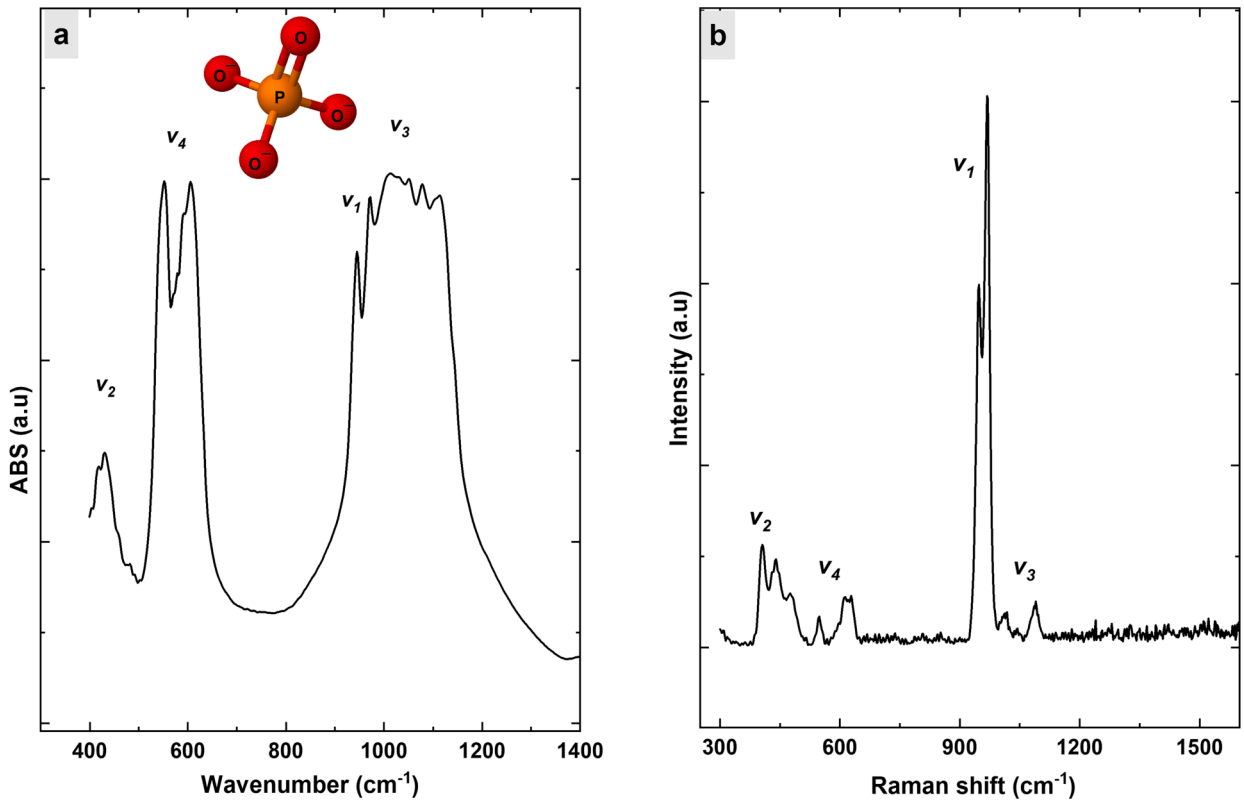

Fig. 5. Vibrational spectra of β-TCP. a) IR spectrum and b) Raman spectrum.

Table 2
List of observed and reported infrared (IR) and Raman (R) bands of β-TCP in comparison to the calculated bands of the free PO_4^{3-} ion in cm^{-1}.

Vibration modes	Observed		Reported		Calculated vibrational bands of free PO_4^{3-} [61,63]
	IR	R	IR [58,61]	R [60,62]	
ν_1	945, 972, 995	948, 968	946, 960, 961, 975	946–949, 961, 970	938, 937 (R active)
ν_2	408, 424, 433	406, 438, 476	472, 460, 435, 436	405, 439, 475, 483	420, 358 (R active)
ν_3	1013, 1029, 1051, 1078	1014, 1090	1036, 1093, 1000–1100	1005, 1031, 1074, 1091	1017, 1080 (IR and R active)
ν_4	550, 670, 605	548, 610, 628	565, 602, 560–600	547–631, 549, 612	567, 500 (IR and R active)

According to factor group calculations, 378 frequency modes are expected in β-TCP. These modes correspond to the internal vibrations of the 42 phosphate tetrahedra accommodated in the unit cell. However, not all bands are observable due to the overlapping of the modes in a narrow energy range [60]. As detailed in Table 2, the vibrational modes of the free ion are not always active in the IR and Raman regions. While in the solid state, all four modes are visible in both regions due to band splitting. Shifts in energy up to 30 cm^{-1} (Table 2) were identified in the recorded spectra with respect to the free ion, this can be ascribed to the crystallographic distortion of phosphate tetrahedra in β-TCP. This distortion is caused by the surrounding cations (Ca^{+2}) as mentioned above and it is corelated to the site and group symmetry effects [60].

3.5. SEM, EDS and ICP-OES elemental analyses of β-TCP

The microstructure and chemical composition of the prepared materials were examined using SEM-EDS. Fig. 6 below shows (a) micrograph of the β-TCP and (b) the elemental maps obtained from the EDS analysis. The elemental concentration is presented in atomic percentage basis (At%). From the SEM micrograph (Fig. 6a), it is evident that the synthesized β-TCP particles are similar in size and morphology. The hexagonal nature of the grains is obvious along the edges and their size range from 1–5 μm. It is worth mentioning that these morphological characteristics of β-TCP can vary depending on the preparation method [64].

From the elemental maps of Fig. 6b, no impurities were observed and only Ca, P and O were identified. The distribution of these elements was found to be even over the mapped area and the determined Ca/P ratio was 1.55. Nevertheless, SEM-EDS is generally considered as a semi-quantitative technique. Thus, ICP-OES measurements were performed to accurately determine the bulk elemental composition and the Ca/P ratio in the pure samples. From the measurements, the determined molar Ca/P ratio was 1.507 ± 0.006, that agrees with the stoichiometric value and no other impurities were detected. This can be attributed to the use of high purity starting materials.

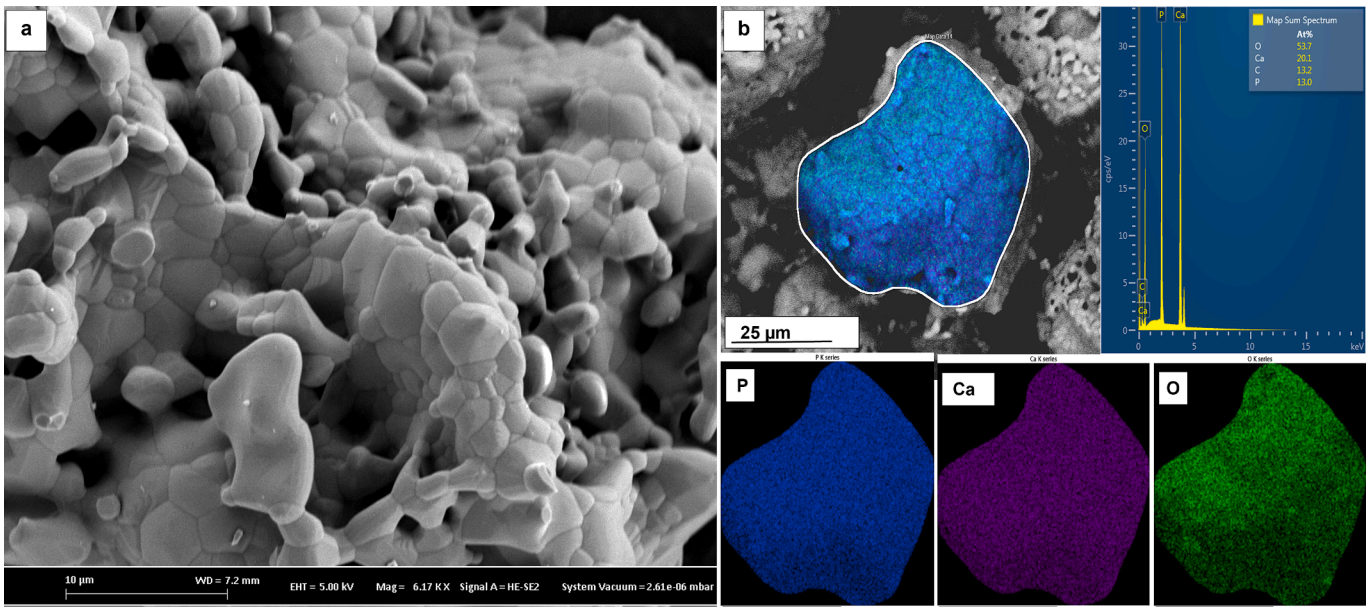

Fig. 6. A) FE-SEM image (BSE) and b) EDS mapping of the elemental distribution in the sample.

3.6. Reproducibility

The reproducibility of the three-stage solid state method was examined by preparing three replicates. The purity of these replicates was determined by the Rietveld analysis to be > 99 %, as previously discussed in Table 1. Fig. 7 below shows the XRD patterns of these replicates produced using the above-described synthesis procedure in comparison to the standard pattern (PDF Card No.01–090-0977) [50]. The purity of these samples was also examined using the other techniques described herein. The results from these techniques indicated that the samples are reproducible and the variations between the obtained data were negligible.

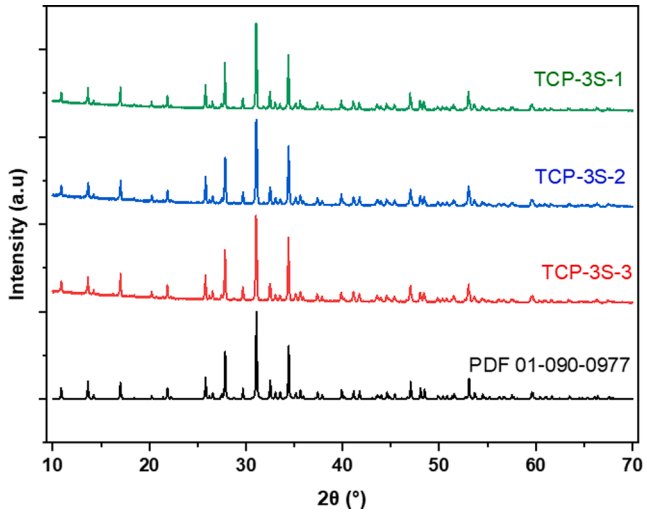

Fig. 7. XRD patterns of standard PDF Card No.01-090-0977 and the β-TCP replicates prepared using the three-stage solid state synthesis.

4. Conclusion

High-purity > 99 % β-TCP was successfully prepared via thermodynamic modelling assisted three-stage solid state method. The thermodynamic modelling was introduced in this work as a powerful tool to investigate the reaction pathways in the synthesis of β-TCP. Also, the calculations enable the prediction of the temperature range at which high purity material can be achieved. This ability is one example of the advantages of using thermodynamic modelling prior to experimental synthesis design of materials. Moreover, the influence of various synthesis parameters on the quality of the final product were thoroughly studied. Experimentally, a single pure phase of β-TCP was obtained at 1000 °C in excellent agreement with the thermodynamic calculations. Detailed characterization using XRD, Rietveld refinement, vibrational spectroscopy, morphology, and the chemical composition confirmed the high purity of the materials. The ICP-OES revealed that the actual Ca/P ratio in the synthesized β-TCP powders is 1.507 ± 0.006. The reproducibility of the material was scrutinized and the variation among the analysed replicates was negligible. The three-stage synthesis design reported here minimized the presence of common secondary phases that are typically correlated with β-TCP synthesis. This design can be implemented to obtain high quality β-TCP material for use in different applications and studies.

CRediT authorship contribution statement

Sana Elbashir: Conceptualization, Methodology, Investigation, Formal analysis, Validation, Visualization, Writing – original draft. **Markus Broström:** Conceptualization, Supervision, Writing – review & editing. **Nils Skoglund:** Conceptualization, Supervision, Funding acquisition, Writing – review & editing.

Declaration of competing interest

The authors declare that they have no known competing financial interests or personal relationships that could have appeared to influence

the work reported in this paper.

Data availability

Data will be made available on request.

Acknowledgements

The Swedish Research Council (Grant no 2017-05331); and Formas (Grant no 2017-01613) are gratefully acknowledged for the financial support of this work. Further, the authors acknowledge the support from Bio4Energy; Vibrational Spectroscopy Core Facility at Chemical Biological Centre (KBC), Umeå University; and Umeå Core Facility for Electron Microscopy (UCEM) at the Chemical Biological Centre (KBC), Umeå University, part of the National Microscopy Infrastructure, NMI (VR-RFI 2016-00968).

References

[1] L. Vaiani, A. Boccaccio, A.E. Uva, G. Palumbo, A. Piccininni, P. Guglielmi, S. Cantore, L. Santacroce, I.A. Charitos, A. Ballini, Ceramic materials for biomedical applications: an overview on properties and fabrication processes, J. Funct. Biomater. 14 (3) (2023) 146.
[2] S.K. Kucko, S.M. Raeman, T.J. Keenan, Current advances in hydroxyapatite- and β-tricalcium phosphate-based composites for biomedical applications: a review, Biomed. Materi. Devices 1 (1) (2023) 49–65.
[3] H. Budharaju, S. Suresh, M.P. Sekar, B. De Vega, S. Sethuraman, D. Sundaramurthi, D.M. Kalaskar, Ceramic materials for 3D printing of biomimetic bone scaffolds – current state-of-the-art & future perspectives, Mater. Des. 231 (2023) 112064.
[4] S. Chand, R. Mehra, V. Chopra, Recent advancements in calcium based phosphate materials for luminescence applications, J. Lumin. 252 (2022) 119383.
[5] F.N. Depboylu, P. Korkusuz, E. Yasa, F. Korkusuz, Smart bioceramics for orthopedic applications, Innovative Bioceramics in Translational Medicine II: Surgical Applications (2022) 157-186.
[6] S.V. Dorozhkin, P.R. Young, Chapter 7 - Calcium phosphates in geological, biological, and industrial systems, in: Z. Amjad, K.D. Demadis (Eds.), Water-Formed Deposits, Elsevier2022, pp. 141-165.
[7] X. Hou, L. Zhang, Z. Zhou, X. Luo, T. Wang, X. Zhao, B. Lu, F. Chen, L. Zheng, Calcium phosphate-based biomaterials for bone repair, J. Funct. Biomater. 13 (4) (2022) 187.
[8] Q. Liu, J.H. Kim, M. Cho, S.H. Kim, B. Xu, S. Amirthalingam, N.S. Hwang, J.H. Lee, Bioactive magnesium-based whitlockite ceramic as bone cement additives for enhancing osseointegration and bone regeneration, Mater. Des. 229 (2023) 111914.
[9] A. Gaikwad, Y.R. Parauha, S. Dhoble, K. Dabre, Development of colour tunable phosphor via rare earth doping in eulytite type Ba3Bi2 (PO4) 4 host material, J. Mater. Sci. Mater. Electron. 34 (20) (2023) 1521.
[10] C. Nandanwar, N. Kokode, A. Yerpude, S. Dhoble, Effect of dopant concentration on luminescence properties of Ba3 (PO4) 2: RE (RE= Sm3+, Eu3+, Dy3+) phosphor for solid-state lighting, Chem. Data Collect. 43 (2023) 100979.
[11] N. Lyczko, A. Nzihou, P. Sharrok, Calcium phosphate sorbent for environmental application, Procedia Eng. 83 (2014) 423–431.
[12] M. Kalbarczyk, A. Szcześ, D. Sternik, The preparation of calcium phosphate adsorbent from natural calcium resource and its application for copper ion removal, Environ. Sci. Pollut. Res. 28 (2) (2021) 1725–1733.
[13] J. Enax, F. Meyer, E. Schulze Zur Wiesche, M. Epple, On the application of calcium phosphate micro- and nanoparticles as food additive, Nanomaterials (basel) 12 (22) (2022).
[14] F.J. Carmona, A. Guagliardi, N. Masciocchi, Nanosized calcium phosphates as novel macronutrient nano-fertilizers, Nanomaterials (basel) 12 (15) (2022).
[15] G. Trömel, W. Fix, Investigation in the calcium oxide-phosphoric acid system, Arch. Eisenhuttenwes 32 (4) (1961) 209–212.
[16] M.C. Tronco, J.B. Cassel, L.A. dos Santos, α-TCP-based calcium phosphate cements: a critical review, Acta Biomater. 151 (2022) 70–87.
[17] K.S. TenHuisen, P.W. Brown, Phase evolution during the formation of α-tricalcium phosphate, J. Am. Ceram. Soc. 82 (10) (1999) 2813–2818.
[18] J.M. Hughes, B.L. Jolliff, J. Rakovan, The crystal chemistry of whitlockite and merrillite and the dehydrogenation of whitlockite to merrillite, 93(8-9) (2008) 1300-1305.
[19] A.A. Belik, F. Izumi, T. Ikeda, B.I. Lazoryak, V.A. Morozov, A.P. Malakho, S. Y. Stefanovich, V.V. Grebenev, O.V. Shelmenkova, T. Kamiyama, K. Oikawa, I. A. Leonidov, O.N. Leonidova, S.A. Davydov, Structural changes and phase transitions in whitlockite-like phosphates, Phosphorus Sulfur Silicon Relat. Elem. 177 (6–7) (2002) 1899–1902.
[20] N. Somers, F. Jean, M. Lasgorceix, N. Preux, C. Delmotte, L. Boilet, F. Petit, A. Leriche, Fabrication of doped β-tricalcium phosphate bioceramics by Direct Ink Writing for bone repair applications, J. Eur. Ceram. Soc. 43 (2) (2023) 629–638.
[21] D.F. Macedo, A.F. Cunha, J.F. Mano, M.B. Oliveira, A.P. Silva, Tricalcium phosphate doped with Mg2+ and combinations of Mn2+, Zn2+ and Fe3+: a DoE study on sintering, mechanical, microstructural and biological properties, Ceram. Int. 48 (14) (2022) 20467–20477.
[22] N. Somers, F. Jean, M. Lasgorceix, G. Urruth, S. Balvay, C. Gaillard, L. Gremillard, A. Leriche, Mg2+, Sr2+, Ag+, and Cu2+ co-doped β-tricalcium phosphate: improved thermal stability and mechanical and biological properties, J. Am. Ceram. Soc. 106 (7) (2023) 4061–4075.
[23] R. Yao, Y. Zhao, S. Han, R. Shan, L. Liu, Y. Sun, X. Yao, X. Wang, R. Hang, Microstructure, mechanical properties, in vitro degradation behavior and in vivo osteogenic activities of Zn-1Mg-β-TCP composites for bone defect repair, Mater. Des. 225 (2023) 111494.
[24] M.M. Ferreira, A.F. Brito, D. Brazete, I.C. Pereira, E. Carrilho, A.M. Abrantes, A. S. Pires, M.J. Aguiar, L. Carvalho, M.F. Botelho, J.M.F. Ferreira, Doping β-TCP as a strategy for enhancing the regenerative potential of composite β-TCP-alkali-free bioactive glass bone grafts. experimental study in rats, Materials (basel) 12 (1) (2018).
[25] D. Liu, L. Dong, H. Wang, J. Bai, J. Shi, W. Chen, H. Yan, B. Li, H. Sun, S. Chen, Amorphous iron-calcium phosphate-mediated biomineralized scaffolds for vascularized bone regeneration, Mater. Des. 235 (2023) 112413.
[26] Y. Pan, J.L. Huang, C.Y. Shao, Preparation of β-TCP with high thermal stability by solid reaction route, J. Mater. Sci. 38 (5) (2003) 1049–1056.
[27] J.S. Cho, D.S. Jung, J.M. Han, Y.C. Kang, Nano-sized α and β-TCP powders prepared by high temperature flame spray pyrolysis, Mater. Sci. Eng. C 29 (4) (2009) 1288–1292.
[28] K. Sanosh, M.-C. Chu, A. Balakrishnan, T. Kim, S.-J. Cho, Sol–gel synthesis of pure nano sized β-tricalcium phosphate crystalline powders, Curr. Appl Phys. 10 (1) (2010) 68–71.
[29] S.C. Liou, S.Y. Chen, Transformation mechanism of different chemically precipitated apatitic precursors into β-tricalcium phosphate upon calcination, Biomaterials 23 (23) (2002) 4541–4547.
[30] J. Ando, Tricalcium phosphate and its variation, Bull. Chem. Soc. Jpn 31 (2) (1958) 196–201.
[31] S.V. Dorozhkin, Bioceramics of calcium orthophosphates, Biomaterials 31 (7) (2010) 1465–1485.
[32] L. Sha, Y. Liu, Q. Zhang, M. Hu, Y. Jiang, Microwave-assisted co-precipitation synthesis of high purity β-tricalcium phosphate crystalline powders, Mater. Chem. Phys. 129 (3) (2011) 1138–1141.
[33] M.-H. Hong, J.H. Lee, H.S. Jung, H. Shin, H. Shin, Biomineralization of bone tissue: calcium phosphate-based inorganics in collagen fibrillar organic matrices, Biomaterials Research 26 (1) (2022) 42.
[34] M. Descamps, J.C. Hornez, A. Leriche, Effects of powder stoichiometry on the sintering of β-tricalcium phosphate, J. Eur. Ceram. Soc. 27 (6) (2007) 2401–2406.
[35] A.P. Oliveira, M. Motisuke, C.V. Leal, M.M. Beppu, A comparative study between β-TCP prepared by solid state reaction and by aqueous solution precipitation: application in cements, Key Eng. Mater. 361–363 (2008) 355–358.
[36] A. Indurkar, R. Choudhary, K. Rubenis, J. Locs, Advances in sintering techniques for calcium phosphates ceramics, Materials (basel) 14 (20) (2021).
[37] R. Rahmani, S.I. Lopes, K.G. Prashanth, Selective laser melting and spark plasma sintering: a perspective on functional biomaterials, J. Funct. Biomater. 14 (10) (2023) 521.
[38] F. Zhang, J. Yang, Y. Zuo, K. Li, Z. Mao, X. Jin, S. Zhang, H. Gao, Y. Cui, Digital light processing of β-tricalcium phosphate bioceramic scaffolds with controllable porous structures for patient specific craniomaxillofacial bone reconstruction, Mater. Des. 216 (2022) 110558.
[39] J.H. Welch, W. Gutt, 874. High-temperature studies of the system calcium oxide-phosphorus pentoxide, J. Chem. Soc. (resumed) (1961) 4442–4444.
[40] M. Canillas, P. Pena, A.H. De Aza, M.A. Rodríguez, Calcium phosphates for biomedical applications, Bol. SECV 56 (3) (2017) 91–112.
[41] C.W. Bale, P. Chartrand, S. Degterov, G. Eriksson, K. Hack, R.B. Mahfoud, J. Melançon, A. Pelton, S. Petersen, FactSage thermochemical software and databases, Calphad 26 (2) (2002) 189–228.
[42] C.W. Bale, E. Bélisle, P. Chartrand, S.A. Decterov, G. Eriksson, A.E. Gheribi, K. Hack, I.H. Jung, Y.B. Kang, J. Melançon, A.D. Pelton, S. Petersen, C. Robelin, J. Sangster, P. Spencer, M.A. Van Ende, FactSage thermochemical software and databases, 2010–2016, Calphad 54 (2016) 35–53.
[43] E. Yazhenskikh, T. Jantzen, K. Hack, M. Muller, A new multipurpose thermodynamic database for oxide systems, Расплавы 2 (2019) 116–124.
[44] M. Yashima, A. Sakai, T. Kamiyama, A. Hoshikawa, Crystal structure analysis of β-tricalcium phosphate Ca3(PO4)2 by neutron powder diffraction, J. Solid State Chem. 175 (2) (2003) 272–277.
[45] A. Pardo, J. Romero, E. Ortiz, High-temperature behaviour of ammonium dihydrogen phosphate, J. Phys. Conf. Ser. 935 (1) (2017) 012050.
[46] J. Zhu, G.L. Riskowski, R.I. Mackie, A laboratory study on metal corrosion by ammonia gas, Transactions of the ASAE 42 (3) (1999) 783–788.
[47] S. Gates-Rector, T. Blanton, The powder diffraction file: a quality materials characterization database, Powder Diffr. 34 (4) (2019) 352–360.
[48] B. Axs, DIFFRACplus EVA 10.0 Release 2004, Germany, Bruker AXS, 2004.
[49] A. Coelho, DIFFRACplus TOPAS 4.2, BrukerAXS GmbH, Karlsruhe, 2008.
[50] S. Liu, Y. Liang, X. Ma, H. Li, W. Zhang, D. Tu, Y. Chen, Tunable photoluminescence and energy transfer efficiency in β-Ca3(PO4)2-Ca9La(PO4)7: Eu2+, Mn2+ solid solution phosphors introduced by emptying site and structural confinement effect for solid-state lighting application, Inorg. Chem. 59 (6) (2020) 3596–3605.
[51] I.T. Trabelsi, A. Oueslati, T. Mhiri, M. Toumi, Synthesis, characterization and ionic conductivity of Ca8− xSrxBi2 (PO4) 6O2 for x={3, 4, 5}, J. Alloy. Compd. 641 (2015) 14–21.

[52] A.C. Tas, X-ray diffraction data for flux-grown calcium hydroxyapatite whiskers, Powder Diffr. 16 (2) (2001) 102–106.
[53] N. Webb, R. Marsh, The crystal and molecular structure of bisindenylruthenium, Acta Crystallogr. 22 (3) (1967) 382–387.
[54] J. Rajaram, J.C. Kuriacose, Kinetics and Mechanisms of Chemical Transformations, Macmillan Publishers India Limited, 2000.
[55] R. Röttger, H. Schmalzried, Chemical kinetics at solid/solid interfaces, Solid State Ion. 150 (1) (2002) 131–141.
[56] A.R. West, Solid State Chemistry and Its Applications, Wiley India Pvt, Limited, 2007.
[57] B.H. Toby, R factors in rietveld analysis: how good is good enough? Powder Diffr. 21 (1) (2006) 67–70.
[58] B.-C. Liga, B. Natalija, Research of Calcium Phosphates Using Fourier Transform Infrared Spectroscopy, in: T. Theophile (Ed.), Infrared Spectroscopy, IntechOpen, Rijeka, 2012, p. Ch. 6.
[59] K. Nakamoto, Infrared and Raman Spectra of Inorganic and Coordination Compounds, Handbook of Vibrational Spectroscopy, 2001.
[60] P.N. de Aza, C. Santos, A. Pazo, S. de Aza, R. Cuscó, L. Artús, Vibrational properties of calcium phosphate compounds. 1. raman spectrum of β-tricalcium phosphate, Chem. Mater. 9 (4) (1997) 912–915.
[61] W. Jastrzębski, M. Sitarz, M. Rokita, K. Bułat, Infrared spectroscopy of different phosphates structures, Spectrochim. Acta A Mol. Biomol. Spectrosc. 79 (4) (2011) 722–727.
[62] P.N. de Aza, F. Guitián, C. Santos, S. de Aza, R. Cuscó, L. Artús, Vibrational properties of calcium phosphate compounds. 2. comparison between hydroxyapatite and β-tricalcium phosphate, Chem. Mater. 9 (4) (1997) 916–922.
[63] A. Jillavenkatesa, R.A. Condrate, The infrared and raman spectra of β-and α-tricalcium phosphate (Ca3(Po4)2), Spectrosc. Lett. 31 (8) (1998) 1619–1634.
[64] C. Ruiz-Aguilar, U. Olivares-Pinto, E.A. Aguilar-Reyes, R. López-Juárez, I. Alfonso, Characterization of β-tricalcium phosphate powders synthesized by sol–gel and mechanosynthesis, Boletín De La Sociedad Española De Cerámica y Vidrio 57 (5) (2018) 213–220.